SUPPRESSION OF ASPHALTENE ADSORPTION AND DEPOSITION IN POROUS MEDIA

Harrison Sarsito

A thesis

submitted in partial fulfillment of the

requirements for the degree of

Master of Science in Chemical Engineering

University of Washington

2021

Committee:

John C. Berg (Advisor)

David Bergsman

Program Authorized to Offer Degree:

Chemical Engineering

University of Washington

SUPPRESSION OF ASPHALTENE ADSORPTION AND DEPOSITION IN POROUS MEDIA

Harrison Sarsito

Chair of the Supervisory Committee:

John C. Berg

Rehnberg Professor of Chemical Engineering

Department of Chemical Engineering

Abstract

Asphaltenes constitute a polar and aromatic class of molecules that are part of bitumen, the heaviest component of crude oil. During crude oil extraction and refining, the precipitation and deposition of these asphaltenes result in numerous upstream and downstream problems, such as well-bore clogging and poisoning of refinery catalysts. This study investigates the usage of surface modification techniques to reduce the extent of asphaltene adsorption and deposition under dynamic conditions and high pressures. UV-Vis spectroscopy and differential pressure measurements are used to quantify the extents of asphaltene adsorption and deposition on both treated and untreated silica surfaces. Perfluorinated silanes were found to be most effective in reducing the extent of asphaltene adsorption/deposition on silica surfaces. A complimentary quartz crystal microbalance study was also conducted to investigate asphaltene deposition.

1. Introduction

Asphaltenes are the largest, densest, most polar and surface fraction of oil generally defined by a solubility regime: soluble in aromatic solvents such as toluene and benzene but not in alkanes such as n-alkanes [1]. They are defined by this solubility class due to the convenient way in which asphaltenes are extracted from crude oil, and the difficulties in the general characterization of their molecular properties [2]. Historically, there has been debate on the molecular structures of asphaltenes, but the recent development of advanced analytical techniques such as high-resolution Fourier transform ion cyclotron resonance mass spectroscopy (FT-ICR MS) has granted deeper insight into their structures. While the exact structures of asphaltenes vary depending on their source, their molecular weight averages around 750 g/mol. Asphaltene molecules are often characterized as having a polyaromatic core with aliphatic groups attached to its core. This core contains heteroatoms such as N, O and S, and sometimes even metals such as Vanadium, Nickel and Iron [3–5]. Due to these various chemical functionalities, asphaltene molecules are known to have different association mechanisms such as $\pi - \pi$ interactions of their aromatic cores, acid-base interactions through the oxygen/nitrogen-containing chains, metal complex formation through the transition metal functionality, and lastly van der Waals forces from the hydrophobic pockets [6]. These intermolecular forces drive the formation of asphaltene aggregates, a phenomenon best described by the Yen-Mullins model [7].

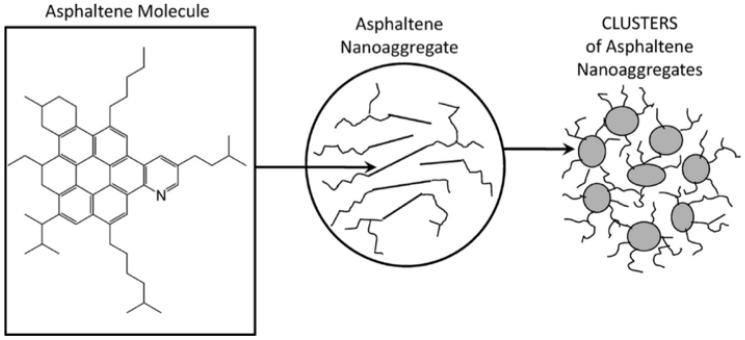

Figure 1: Yen-Mullins model for asphaltene morphology in solution[7]

The Yen Mullins Model describes the two-stage stepwise aggregation process of asphaltenes from individual molecules to clusters of nanoaggregates. Individual asphaltene molecules self-assemble into asphaltene nanoaggregates until the solution reaches the critical nanoaggregate concentration (CNAC), after which further nanoaggregate formation stops. The onset of the formation of these asphaltene nanoaggregates/clusters depend on the source of asphaltenes, the solvent and the physical conditions of the system. In toluene, initiation of asphaltene nanoaggregation occurs at a concentration as low as 50 mg/L. These asphaltene nanoaggregates have aggregation numbers of ~6 and sizes of about 2 nm [8]. Ultrasonic studies have shown that the CNAC for asphaltene in toluene occurs around 100 mg/L [9]. Above the CNAC, nanoaggregate growth halts, and these nanoaggregates further associate into clusters of nanoaggregates. These clusters of nanoaggregates are fractal in their scaling, and have aggregation numbers of ~8, with sizes of 3 – 10 nm [10]. These clusters of nanoaggregates are not to be confused with flocks, which are larger undissolved entities in the micrometer size range formed as a result of continued aggregation during the onset of asphaltene precipitation.

During the crude oil extraction and refining processes, changes in pressure, temperature and oil composition contribute to a destabilization of asphaltenes, causing them to precipitate and deposit in both upstream and downstream processes. The problems that arise due to this deposition include but are not limited to decreases in the volumetric flow in the wellbore regions and pipelines due to clogging of capillaries [11], reductions in oil extraction efficiency due to alterations in the wettability of reservoir rocks [12],and poisoning of catalysts involved in oil refining [13]. Therefore, numerous studies have been centered around understanding the interactions of asphaltenes with solid surfaces and the potential strategies to mitigate their deposition.

The rate and extent of asphaltene adsorption onto solid surfaces is a complex process that is sensitive to many variables such as source of asphaltenes, quality of the solvent and properties of the adsorbent. Researchers have employed a variety of experimental techniques to characterize asphaltene adsorption such as contact angle measurements [14,15], NIR/UV-Vis spectroscopy [16–18], quartz crystal microbalance gravimetry [19,20], ellipsometry and electrokinetic measurements [21,22]. The source of asphaltenes determines the chemical functionalities of the asphaltene molecules, which impact the extent of asphaltene adsorption on the same adsorbents. Two studies, conducted by Pernyeszi and Marczerski, may be used to highlight how these geographic differences result in different adsorption behavior onto various clay minerals [23,24]. Both researchers studied the static adsorption of asphaltenes dissolved in toluene into different clay minerals, such as kaolinite, illite and montmorillonite, using UV-Vis spectroscopy. Pernyeszi observed that the adsorption behavior of Hungarian asphaltenes onto Kaolinite exhibited Langmuir behavior, while Marczewski observed asserted that the adsorption of Polish asphaltenes onto the same material exhibit "initial lines of Freundlich character", suggesting lateral interactions and multilayer formation. The quality of solvent and resulting solubility of the asphaltene entities also has a significant impact on the quantity of asphaltene adsorbed onto a surface. Elkholm et al. studied the effects of the solution concentration and solvent quality on asphaltene adsorption using a QCM (Quartz Crystal Microbalance) [25]. They observed that adsorption of asphaltene from toluene onto the gold crystal surface of the QCM probe was a function of concentration, and increased continuously as a function of increasing concentration. Similar to what Marczewski observed, Elkholm attributed multilayer formation onto the gold surface to strong asphaltene-asphaltene interactions in toluene[25]. They also investigated asphaltene adsorption onto gold from a heptane-toluene mixture, and observed that a larger extent of adsorption was detected relative to equivalent concentrations of asphaltenes in toluene alone. This larger extent was attributed to the formation and subsequent adsorption of larger supramolecular aggregates. Syunyaev et al. studied the kinetics and extent of asphaltene adsorption onto a series of minerals (e.g. mica, quartz and dolomite)

using near-infrared spectroscopy [18]. They concluded that the chemical composition and structural parameters of the surface were the main factors controlling adsorption kinetics. Moreover, for adsorbents of the same nature, smaller particle sizes (larger contact area) leads to a higher adsorption rates due to higher contacts points per unit volume of adsorbent. These studies show that the rate and extent of asphaltene adsorption is a highly system-specific process.

Modification of the amphiphilicity of solids with various surface treatments have been explored as a strategy for mitigating asphaltene adsorption. Dudášová et al. studied asphaltene adsorption onto different minerals and clays in an investigation of how surface functionality affected asphaltene adsorption [26]. They observed that the extent of asphaltene adsorption was less on hydrophobic surfaces. Since then, many have built upon the findings of this study to elucidate how these hydrophobic functionalizations hinder asphaltene adsorption. Turgman et al. studied asphaltene adsorption onto flat silica surfaces modified with self-assembled monolayers (SAMs) of varying carbon chain lengths[27]. They observed that the effectiveness of these SAMs was dependent on their ability to shield the interaction between the underlying silica substrate and the asphaltene molecules. They asserted that this was dependent on the SAM carbon chain length and the SAM grafting density (number of SAM molecules per unit area). A more recent study by Girard et al., examined the effects of the physicochemical properties of alkane, hydroxyl and fluorinated surfaces on the extent of asphaltene adsorption [28]. They focused on the initial kinetics of asphaltene adsorption using contact angle measurements, long-term adsorption dynamics using the QCM, and the mechanism and morphology of adsorption using atomic force microscopy (AFM). They observed that alkane surfaces delay the initial monolayer formation and result in thicker adsorption layers compared to hydroxyl and fluorinated surfaces. Moreover, they observed that fluorinated surfaces reduce the bonding strength between asphaltene molecules and the underlying substrate, potentially inducing a semi-transient state in which asphaltene molecules are released post-adsorption.

Currently very little work exists in extending these surface modification techniques to asphaltenes in a poor solvent, where there exist clusters of nanoaggregates and even precipitated flocculates. This study attempts to bridge this gap by doing a systematic exploration of how surface modification mitigates the mass of asphaltene adsorbed and deposited onto silica particles under flow conditions. In the literature, the terms “adsorption” and “deposition” have been used interchangeably to describe the asphaltene deposition phenomenon discussed previously. However, in the context of this paper, the two terms are used to describe the accumulation of asphaltene on solid surfaces from different solvents. Asphaltene “adsorption” is used to describe the accumulation of dissolved asphaltene monomers, nanoaggregates or clusters of nanoaggregates onto the silica surface during experiments involving asphaltenes in pure toluene. In contrast, “deposition” is used to describe the accumulation of micrometer-sized asphaltene flocculates or precipitates onto silica, particularly during experiments involving asphaltenes in the 1:1 (w/w) toluene/tetradecane mixture (poor solvent). The silica particles are treated with three types of surfactants: hexadecyl ammonium bromide (HTAB), Pluronic L62® , and 1H, 1H, 2H, 2H – Perfluorodecyltriethoxysilane. Various solutions of asphaltenes in toluene and toluene/tetradecane are pumped through the silica particle packed bed, after which the amount of asphaltene removed in the column per experiment is measured using UV-Vis spectroscopy and differential pressure measurements. In addition, these adsorption/deposition experiments are conducted under dynamic flow conditions and high pressures, to mimic the flow conditions during crude oil extraction.

2. Materials, Experimental Setup and Analysis Methodology

The asphaltenes used in this study were extracted from the West Kuwait Marrat Oil Formation. The extraction procedure involved the precipitation of asphaltenes from the oil by an excess of n-pentane, following the separation procedure described in ASTM D-3279 [29]. Specific constituents of the Marrat Oil are described below in Table 1 below.

Table 1: Marrat Oil Constituents

Sample	Viscosity (cP @ 50ºC)	C (wt. %)	S (wt. %)	N (ppm)	Ni (ppm)	V (ppm)	C5 Asph., (wt.%)	Resin (wt. %)
Marrat Oil	3.50	1.50	1.04	272	0.440	1.41	0.368	0.771

2.1 Material Preparation and Experimental Procedure

Silica Particles. The untreated silica substrate used in these experiments was sand (50-70 mesh) purchased from Sigma-Aldrich. The specific area of the particles was found to be 0.0428 m^2/g as measured using BET surface area analysis, using a FlowSorb II (Micromeritics Corp.; Norcross, GA). The silica particles were effectively dry, with a surface water content of around 20 ppm as measured using Karl-Fischer titration (C20 Coulometric KF Titrator, Mettler Toledo; Columbus, OH).

Asphaltene Solutions. Asphaltene is mixed with pure toluene or 1:1 (by mass) toluene/tetradecane mixture to form a 100 mL asphaltene solution of desired concentration. Toluene (99.8%, anhydrous) was purchased from Sigma-Aldrich. Tetradecane (≥ 95%) was purchased from

Fisher Chemical. The solution is then separated into 20 mL batches. Each batch is sonicated with an output of 60W for 5 min (Sonifier S-250A 250 Analog Ultrasonic Cell Disruptor/Homogenizer, Brandon Ultrasonics; Brookfield, CT). The solutions are then recombined and immediately used for experiment.

Surface Modification of Silica Particles with HTAB. Hexadecyltrimethylammonium bromide or HTAB (≥ 96%) was purchased from Sigma Aldrich. An aqueous surfactant solution of HTAB at its critical micelle concentration was first produced by mixing 0.1092 g of HTAB and 300 mL of distilled water. This concentration approximated the critical micelle concentration of this surfactant in water and was believed to produce a close-packed monolayer on the substrate by electrostatic amphiphilic adsorption[30]. Upon stirring for 1 h, to ensure that all the HTAB was fully dissolved, 24 g of sand particles were added to the mixture. The mixture was then stirred using a magnetic stir bar at a constant rate for 24 h. The silica particles were then filtered and dried at 60ºC overnight.

Surface Modification of Silica Particles with Pluronic L62®. Pluronic L62® (a triblock oligomer made up of 30 propylene oxide monomer subunits between 5 ethylene oxide groups) was purchased from the BASF. For surface modification with Pluronic L62®, 24 g of sand particles were stirred in a mixture of 15 g of Pluronic L62 and 300 mL of water, sufficient to produce a close-packed monolayer[31], over 1 h. The silica particles were then filtered and dried overnight at 60ºC.

Surface Modification of Silica Particles with Fluorinated Silane. The fluorinated silane of choice here is 1H, 1H, 2H, 2H – Perfluorodecyltriethoxysilane (97%), purchased from Sigma-Aldrich. For silane modification, 1 mL of the Perfluorodecyltriethoxysilane was added to a 100 mL 95:5 wt% solution of ethanol and water. Glacial acetic acid, purchased from EMD Chemicals, was added to the

mixture dropwise until the pH of the solution reached 4.5. The silanes were left to hydrolyze in solution over 10 min. 24 g of the silica particles were then added to the mixture, and the resultant solution was left to stir over 1 h. The concentration of the silane was sufficient to produce a close-packed monolayer[32]. The silica particles were filtered and dried overnight at 60ºC.

Flow System Experimental Procedure. The experimental setup is as shown in **Figure 2**. The setup was adapted from what was used by Alkafeef et al. in their study of the electrokinetic potential at reservoir rock surfaces [33]. The silica particles of interest are first packed into a 4-in long, 0.25-in i.d HPLC column, plugged at each end using steel mesh, and connected to the apparatus. A positive displacement pump (Rainin Dynamax SD-200, Agilent; Santa Clara, CA) is then used to pump solvent (the same one used in the asphaltene solution to test) through the system to flush out any trapped air bubbles and to wet the entire apparatus. The solution is pumped at a flow rate of 1 mL/min for a total duration of 90 min. The system pressure is maintained at 100 psi using a back-pressure regulator (U3L Equilibar; Fletcher, NC) to assure that any air pockets in the apparatus would be dissolved. The back-pressure regulator was set at 100 psi using nitrogen gas. The column outlet stream flows through a 1-mm quartz cuvette placed inside an inline UV-Vis spectrometer (Cary 60, Agilent; Santa Clara, CA), which was used to quantify the mass of asphaltene adsorbed in the column for asphaltene adsorption experiments. To quantify the mass of asphaltene adsorbed/deposited in the asphaltene deposition experiments, a differential pressure transducer (DP 15, Validyne; Northridge, CA) was used to measure the column pressure drop to sustain the 1 mL/min flow rate in real time. All experiments were conducted at 22°C.

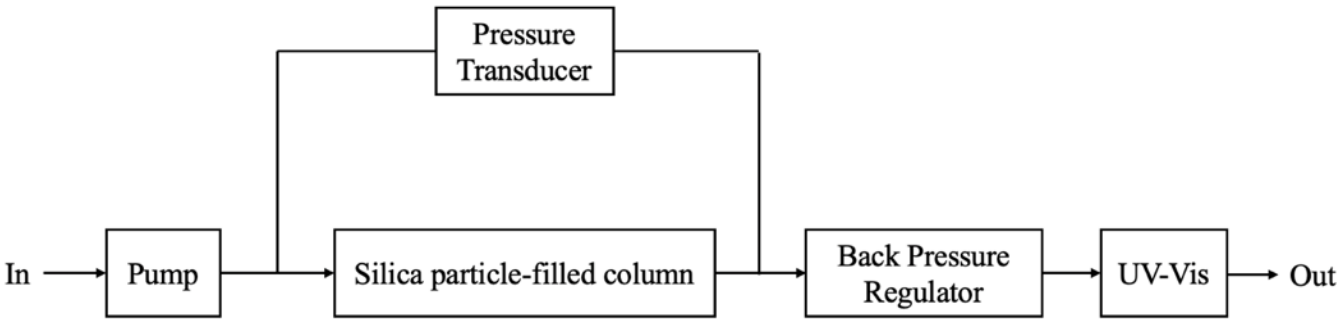

Figure 2: Flow system schematic

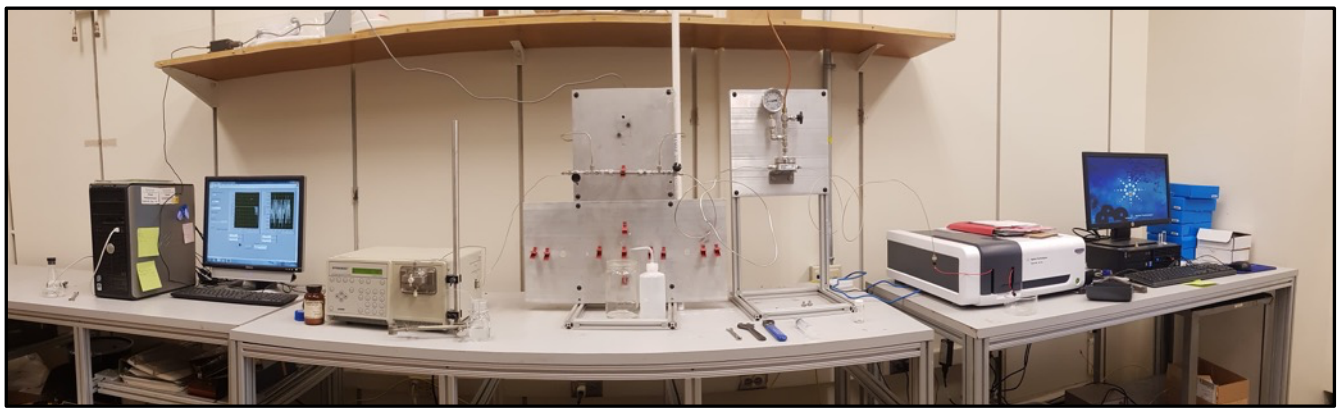

Figure 3: Picture of the flow system

Functionalization of Gold Crystal Surfaces. This functionalization procedure was adapted from Girard et al.[28] The gold/quartz crystals of a quartz crystal microbalance (QCM 200, Stanford Research Systems; Sunnyvale, CA) were modified to exhibit three different surface functionalities[34]. The three surfactants used for surface modification were hexadecanethiol, 2-mercaptoethanol and 1H, 1H, 2H, 2H – Perfluorodecanethiol to impart a hydroxyl, alkane and fluorinated surface functionality on three gold crystals respectively. For each functionalization, the gold crystals were left in a 60 mL, 50 mM mixture of the particular surfactant and 200-proof ethanol for 90 h.

Adsorption/Deposition Measurements using Quartz Crystal Microbalance (QCM)

Experimental Procedure. The QCM was submerged in a 60 mL asphaltene solution of interest for 1.5 h. The asphaltene solutions were made using the procedure listed in the "Asphaltene Solutions" section above.

2.2 Quantification of Mass of Asphaltene Adsorbed using UV-Vis Spectroscopy

UV-Vis spectroscopy was used to characterize the outlet asphaltene concentration during the study of asphaltene adsorption onto silica, where asphaltene is dissolved in pure toluene. The quantification of the total mass of asphaltene that adsorbs onto silica is measured by tracking the change in the outlet asphaltene concentration over the experimental duration. While it is possible to use UV-Vis spectroscopy to calculate the mass of asphaltene deposited in the column during the study of asphaltene deposition (asphaltene in toluene/tetradecane), it proves inaccurate as asphaltene will also deposit on the walls of the quartz cuvette over the duration of the experiment. This renders the outlet concentration measurements to appear larger than what should be observed. Hence, another method of calculating the mass of asphaltene deposited in the column was needed and is the topic of the next section (**Section 2.3**). The following methodology applies solely to the asphaltene adsorption experiments.

The determination of asphaltene concentration in toluene using UV-Vis spectroscopy relies on the principles of the Beer-Lambert Law, where

$$A = \varepsilon C l \tag{1}$$

where A is the absorbance, ε is the molar extinction coefficient, C is the molar concentration of the chemical species, and l is the pathlength[30]. The Beer-Lambert Law suggests that if the pathlength (the

width of our UV-Vis quartz cell) is held constant; then there is a linear relationship between A and C. Absorbance vs concentration calibration curves for wavelengths of 400, 500, 600, and 700 nm were prepared using 0.2, 0.6, 1, 2, 4, 6 and 8 g/L asphaltene/toluene solutions. These measurements were obtained using a 1-mm deep quartz cuvette.

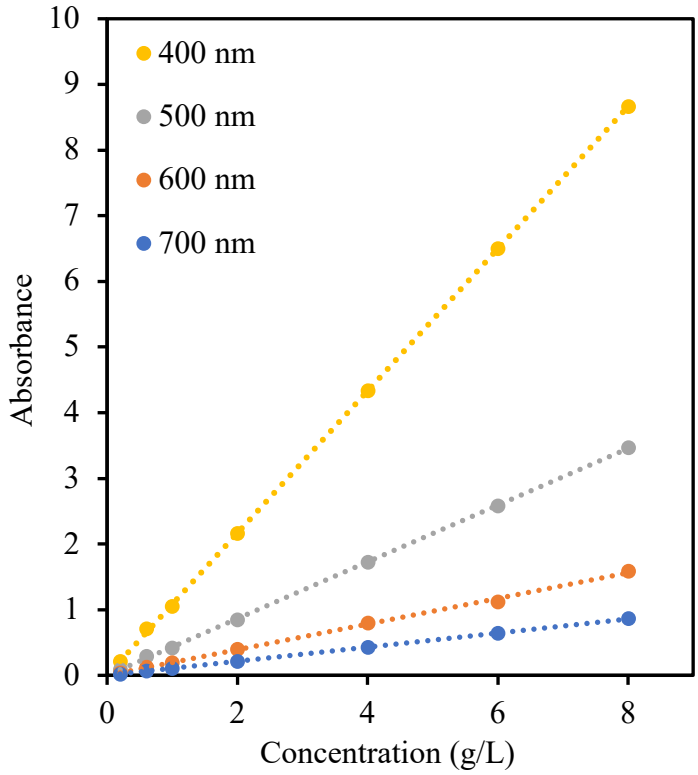

Figure 4: UV-Vis calibration curves for asphaltene in toluene at 22°C

The calibration curves shown in **Figure 3** allow the determination of the linear relationship between A and C

$$A = m_\lambda C \qquad (2)$$

where m_λ denotes the calibration constant for each linear relationship corresponding to a particular wavelength of light. **Table 2** summarizes the values for m_λ obtained for each wavelength through linear regression of each of the calibration curves.

Table 2: Calibration constant m_λ for 400, 500, 600 and 700 nm wavelengths of light

Wavelength (nm)	$\boldsymbol{m_\lambda}$ **(L/g)**
400	1.08
500	0.432
600	0.195
700	0.107

The choice of which wavelength to use to characterize the asphaltene concentration in the column outlet depends on the magnitude of the inlet asphaltene concentration. The measured absorbance through the UV-Vis is the logarithm of the transmission of light through a sample. Transmission is the ratio of the intensity of light transmitted through the sample (I) to the intensity of light transmitted through a blank (I_0).

$$A = \log_{10} T = \log_{10}\left(\frac{I_0}{I}\right) \tag{3}$$

The implication of Eq. (3) is that the useful absorbance range is from 0.1 to 1. Absorbance values greater than or equal to 1 are too high. An absorbance value of 2 suggests that 99% of the available light has been absorbed.

The UV-Vis is set to measure the absorbance of the solution inside the quartz cell (column outlet stream) for the 90-minute experimental duration. Using our empirical relationship defined in Eq. (2), a breakthrough curve for each experiment can be generated. A typical breakthrough curve is shown in **Figure 4** below. It corresponds to a concentration of 6 g/L asphaltene in toluene, adsorbing onto untreated silica.

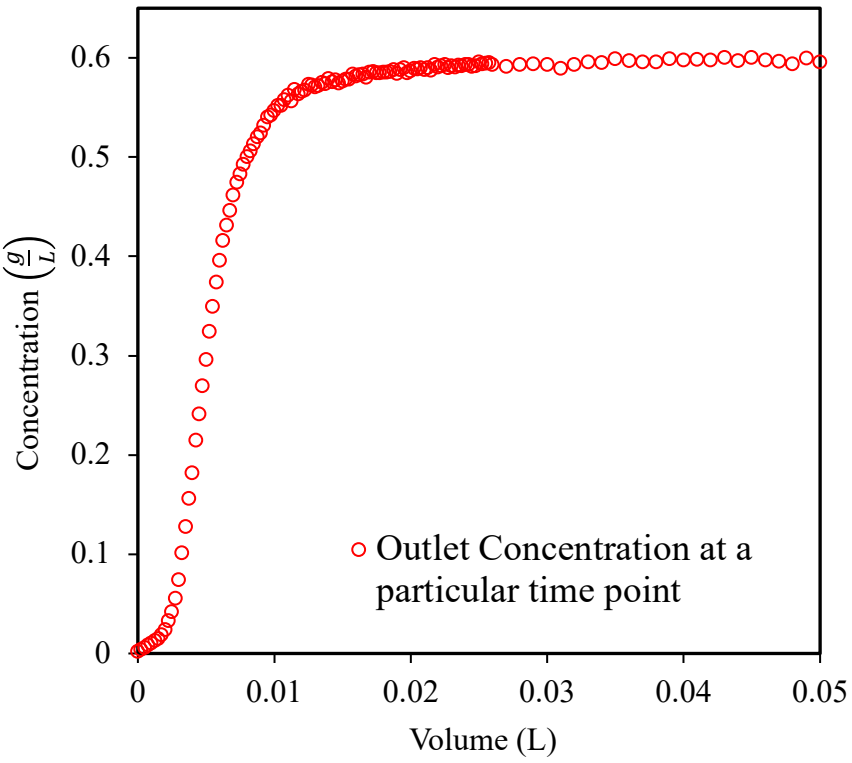

Figure 5: Breakthrough curve for 0.6 g/L asphaltene in toluene trial on untreated silica

Figure 5 suggests that the saturation of the column occurs after approximately 0.02 L of the asphaltene solution has been passed through the column. The shape of this breakthrough curve is representative of all of the other trials across different concentrations and types of silica surfaces. It might be apparent that the points on the breakthrough curve are not evenly spaced apart. This is due to the scan settings implemented on the UV-Vis. From minute 1 to minute 30, the UV-Vis instrument was set to take scans every 1/3 min. After minute 90, it was set to take scans every minute. This is to ensure

that a significant number of points could be obtained when the breakthrough curve starts to slope steeply upward. The adsorbed asphaltene mass, M_{ads} , for each experiment is obtained by calculating the area between the "inlet horizontal" (in this case the horizontal line at 6 g/L) and the breakthrough curve. This was calculated by measuring the difference between two quantities. The first is the product of the inlet concentration and the volume passed through the column in each experiment. As each experiment lasted 90 minutes and used a flow rate of 1 mL/min, the total volume passed through the column in each experiment is 0.09 L. The second is the area between the breakthrough curve and the segment of the X-axis that corresponds to the total volume of solution that was passed through the column in the experiment. This was estimated using a Riemann sum of the concentration measurements from 0 to 0.09 L.

2.3 Quantification of Mass of Asphaltene Adsorbed/Deposited Using the Ergun Analysis

To quantify the mass of asphaltene adsorbed/deposited onto the column during the study of asphaltene deposition, the Ergun analysis was used to relate the changes in the pressure drop across the column to development of an adlayer onto the silica particles. The Ergun equation is typically expressed as

$$\frac{\Delta P}{L} = 150\left(\frac{\mu v_0}{D_p^2}\right)\frac{(1-\varepsilon)^2}{\varepsilon^3} + \frac{7}{4}\left(\frac{\rho v_0^2}{D_p}\right)\frac{(1-\varepsilon)}{\varepsilon} \qquad (4)$$

where ΔP = pressure drop across the column, L = column length, μ = dynamic viscosity of the solution, v_0 = superficial velocity of the liquid, D_p = effective particle diameter, ρ = density of liquid and ε = column porosity[35]. The dynamic viscosity of each solution was determined appropriately during each

trial using a viscometer (Reverse-Flow Cannon-Fenske viscometer Size 50, Fungilab; Haupaugge, NY).

A summarized walkthrough of the Ergun analysis performed on each concentration trial is highlighted in the section below. The complete step-by-step Ergun analysis can be found in **Appendix 1**. The analysis begins with the calculation of the initial porosity (volume ratio of the pores to the volume of the column) of the column, $\varepsilon_{initial}$, which can be determined using the initial mass of the sand packed into the column. The second step is to use the initial pressure difference across the column, $\Delta P_{initial}$, and $\varepsilon_{initial}$ to calculate the average initial diameter of the silica particles, $D_{p,initial}$. Assuming that the asphaltene deposits as a spherical, concentric layer on each silica particle as opposed to as "chunks" that fill the voids in the column, the final column porosity, ε_{final}, and the final diameter of each particle, $D_{p,final}$, can then be expressed in terms of $D_{p,initial}$, $\varepsilon_{initial}$ and the deposited layer thickness, δ. With knowledge of the final pressure drop across the column, δ can be evaluated. The quantity of asphaltene deposited per unit area of the silica particles in the column can also be calculated using the aforementioned quantities and knowledge of the initial mass of silica particles packed into the column in that specific experiment. Post-deposition visual examination of the silica suggest that deposition was at least approximately uniform.

Figure 5 shows the pressure drop data collected for the 6 g/L on untreated silica trial. The shape of this curve is representative of the other curves collected for these deposition experiments. As can be seen, the initial and final pressure drops across the columns can be identified as 0.091 and 0.227 psi respectively. These values are then used in the Ergun analysis as outlined in the previous paragraph and in **Appendix 1**.

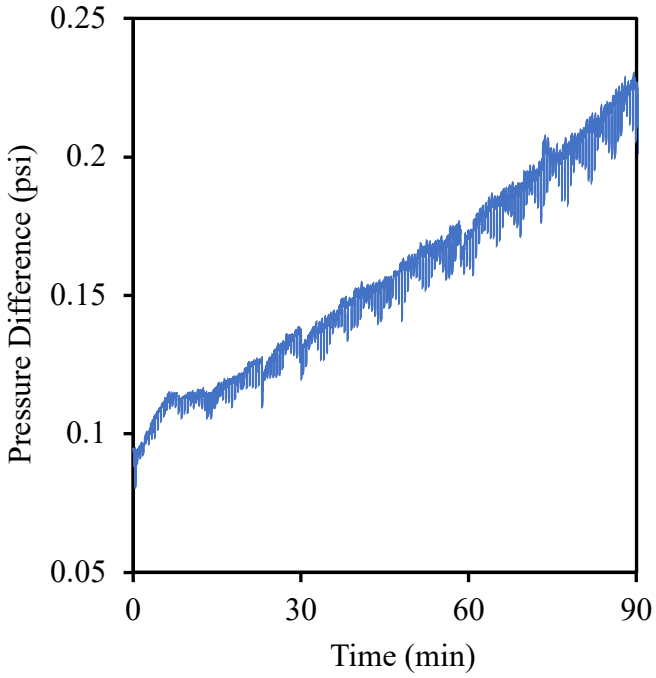

Figure 6: Pressure Drop across the column for 6 g/L deposition experiment on untreated silica

2.4 Quantification of Mass of Asphaltene Adsorbed/Deposited Using QCM

The QCM consists of a gold-plated quartz crystal that oscillates at a very high frequency. When the crystal is placed inside a solution of interest, the change in the oscillating frequency of the crystal is related to the mass adsorbed onto the crystal through the Sauerbrey equation,

$$\Delta \mathrm{m} = -C_f \cdot \Delta f \qquad (5)$$

where C_f is a sensitivity factor, a fundamental property that solely depends on the acousto-elastic properties of the quartz crystal[36]. One of the assumptions of the Sauerbrey equation is that the adsorbed film is a rigid extension of the underlying quartz which does not experience any shear forces during vibration. It also assumes that the adsorbed film is uniform across the quartz crystal.

3. Results and Discussion

3.1 Asphaltene Adsorption Study with Flow System

In our study of asphaltene adsorption, solutions of asphaltene dissolved in pure toluene were run through the flow system apparatus. Asphaltene solution of concentrations between 0.1 and 1 g/L on four silica surfaces. The motivation of conducting this adsorption study is to better understand the asphaltene-solid interactions of the soluble asphaltenes used in this study. The discussion of the experimental results will be prefaced by a brief introduction to the Langmuir and Freundlich adsorption models[30].

3.1.1 Langmuir/Freundlich Adsorption Models

The Langmuir model theorizes that adsorption is restricted to a monolayer. The theory also assumes that there are no lateral adsorbate interactions and the adsorbent possesses surface energetic homogeneity, so that the energy of adsorption does not depend on surface coverage [37]. According to Langmuir theory, Γ, the number of moles (or grams) of solute that adsorbs onto a unit of surface area of the adsorbent can be written as

$$\Gamma = \frac{\Gamma_m(kC)}{1 + kC}, \tag{6}$$

where C is the concentration of the solute (in this case of the asphaltene), k is a constant, and Γ_m is the amount (moles or grams of solute) adsorbed in a close-packed monolayer. Eq. (6) can be rewritten in a linear form,

$$\frac{C}{\Gamma} = \frac{C}{\Gamma_m} + \frac{1}{k\Gamma_m} \ . \qquad (7)$$

If a system can be modelled using Langmuir theory, then a plot of C/Γ vs C from Eq. (7) would yield a straight line with slope $1/\Gamma_m$ and Y-intercept of $1/k\Gamma_m$.

A second model that is often used to describe physical adsorption on these systems is that of Freundlich. The Freundlich model is an empirical model that differs from Langmuir in that it suggests surface energetic heterogeneity, where the energy of adsorption varies exponentially with the extent of surface coverage. The Freundlich model is written as

$$\Gamma = \alpha \mathrm{C}^{\beta}, \qquad (8)$$

where α and β are fitting parameters for each system, with $\beta < 1$. Taking the logarithms of both sides of Eq. (8), the linear form of the Freundlich model can be obtained

$$\log \Gamma = \log \alpha + \beta log C \qquad (9)$$

where the slope will be the value of β and the y-intercept is $\log\alpha$.

3.1.2 Asphaltene Adsorption on Untreated Silica

The mass of asphaltene adsorbed/m^2 of silica surface (Γ) for each asphaltene concentration was obtained using the method outlined in **Section 2.3**, and knowledge of the mass of sand used in each experiment (from which we can determine the total area of sand available for asphaltene adsorption).

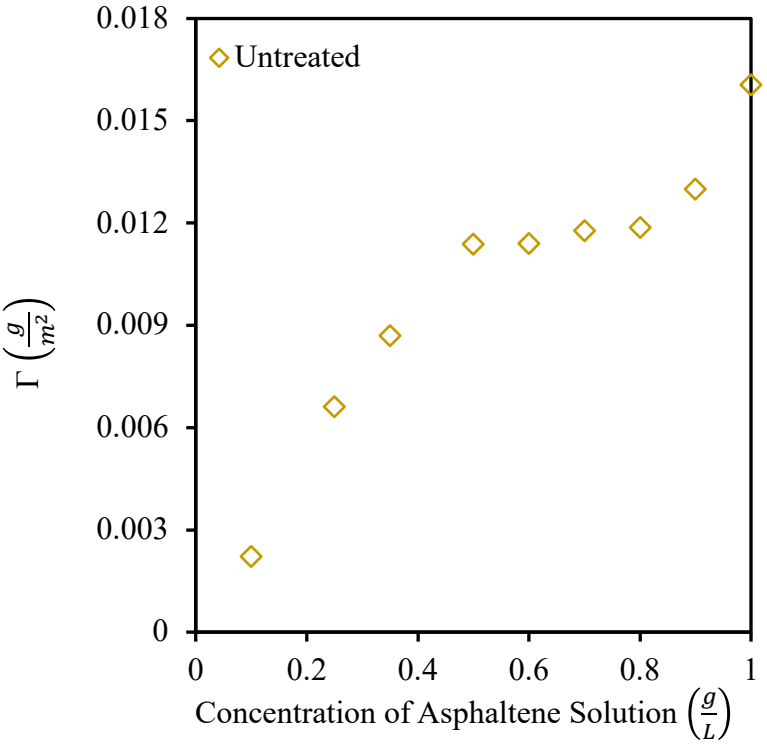

Figure 7: Extent of adsorption onto untreated silica for a concentration range of 0.1 – 1 g/L

The Γ values for each of the ten concentrations on untreated silica is as shown in **Figure 7**. These values appear to increase linearly up to an asphaltene concentration of 0.5 g/L, after which it starts to plateau at a value of 0.012 g/m^2 as the asphaltene concentration is increased further. In terms of magnitude, this is in agreement with that found by other investigators, despite differences in the source of asphaltenes used [19,20,25]. It can be seen that at a concentration of 0.9 g/L, the value of Γ breaks from this plateau and begins to increase. This is suggestive of the formation of a second adsorption layer, which has been observed by other investigators studying asphaltene adsorption, e. g., Acevedo et

al. [38]. They studied adsorption of three different types of asphaltene onto glass surfaces using photothermal surface deformation spectroscopy and concluded that the presence of different asphaltene "entities" (e.g. single asphaltene molecules and asphaltene aggregates) in asphaltene/toluene systems is akin to a mixture containing two surfactants with varying critical micelle concentrations. Not only do these entities have different rates of adsorption, they may also adsorb onto other adsorbed asphaltene species on the silica surface. These multilayers are believed to be the result of the strong acid-base interactions between basic nitrogen with the acidic oxygen groups of the asphaltene entities [39] as well as π- stacking. To simplify the following analysis, the focus will be on the concentration range between 0.1 and 0.8 g/L.

To quantitatively evaluate which model would describe our system more accurately, the adsorption data collected for the untreated silica surface were used to generate two linear plots using Eqs. (7) and (9).

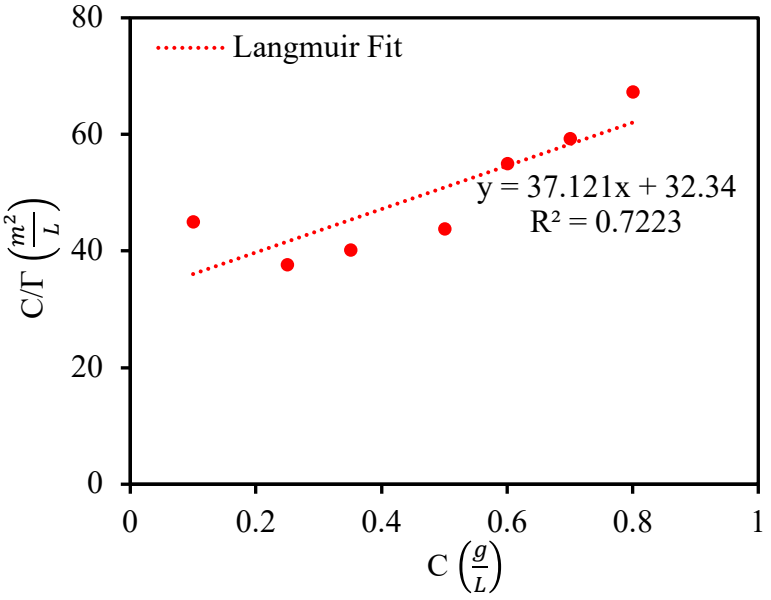

Figure 8: Linear Langmuir model fit to the asphaltene adsorption data on untreated silica

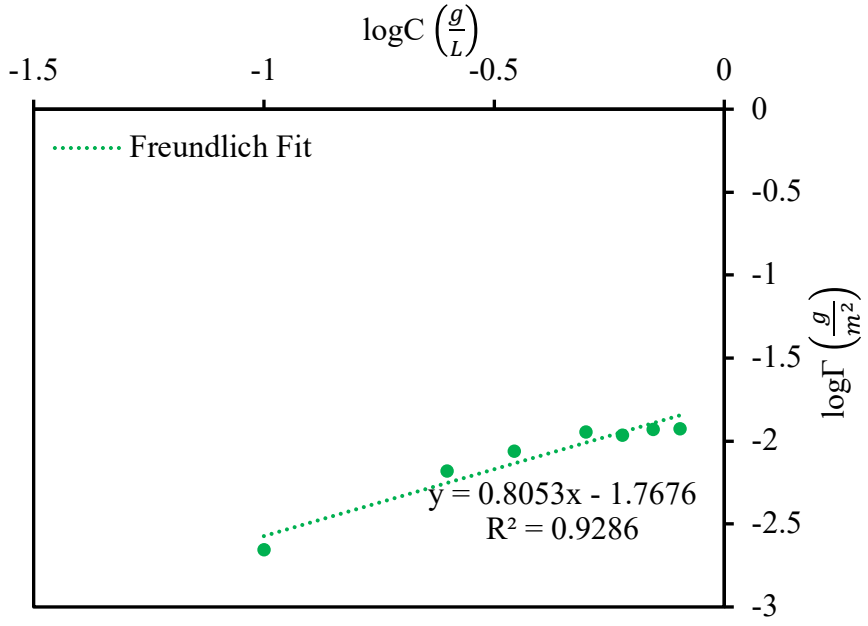

Figure 9: Linear Freundlich model fit to the asphaltene adsorption data on untreated silica

In this concentration range, it can be observed that the Freundlich model fits the data more accurately. The hypothesis here is that even at these low concentration ranges, there are non-negligible attractive interactions between the asphaltene molecules. The Freundlich model can be applied to the data to obtain the adsorption isotherm for this concentration range to obtain the respective α and β values.

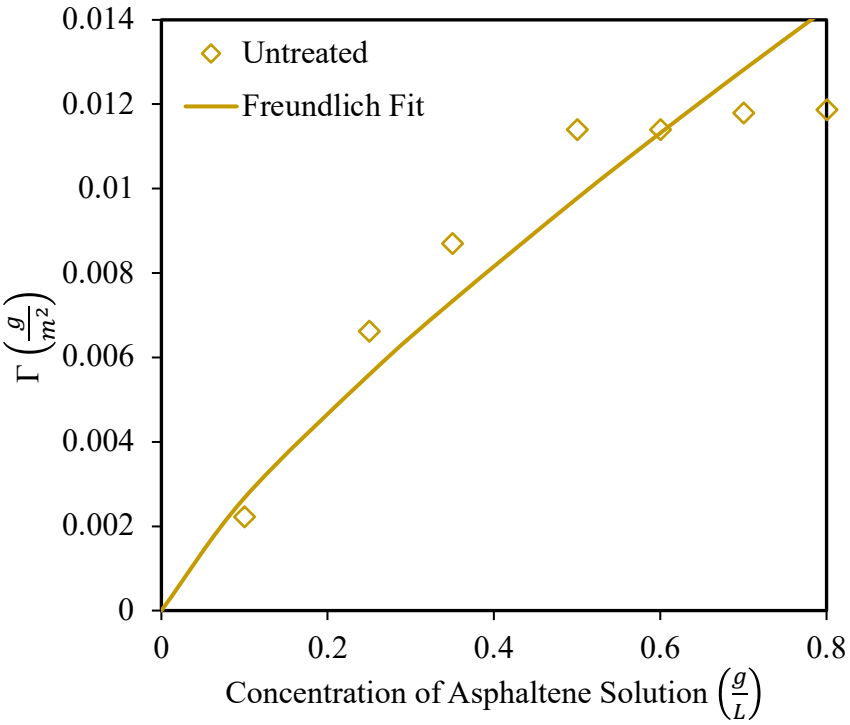

Figure 10: Freundlich model fit for asphaltene adsorption on untreated silica

The Freundlich parameters α and β for this system are 0.017 and 0.81 respectively.

3.1.3 Asphaltene Adsorption on Treated Silica Surfaces

The adsorption experiments involving asphaltene solutions of concentrations between 0.1 and 0.9 g/L were repeated on the three different types of silica surfaces treated with HTAB, Pluronic L62® and 1H, 1H, 2H, 2H – Perfluorodecyltriethoxysilane. HTAB is a quaternary, cationic surfactant with a 16 carbon-long alkane tail. Pluronic L62® is a triblock surfactant bearing a chain of 30 propylene oxide groups sandwiched between 5 ethylene oxide groups on each end. 1H, 1H, 2H, 2H – Perfluorodecyltriethoxysilane is a Q-silane where one of the functional groups is a 1H, 1H, 2H, 2H-Perfluorodecane.

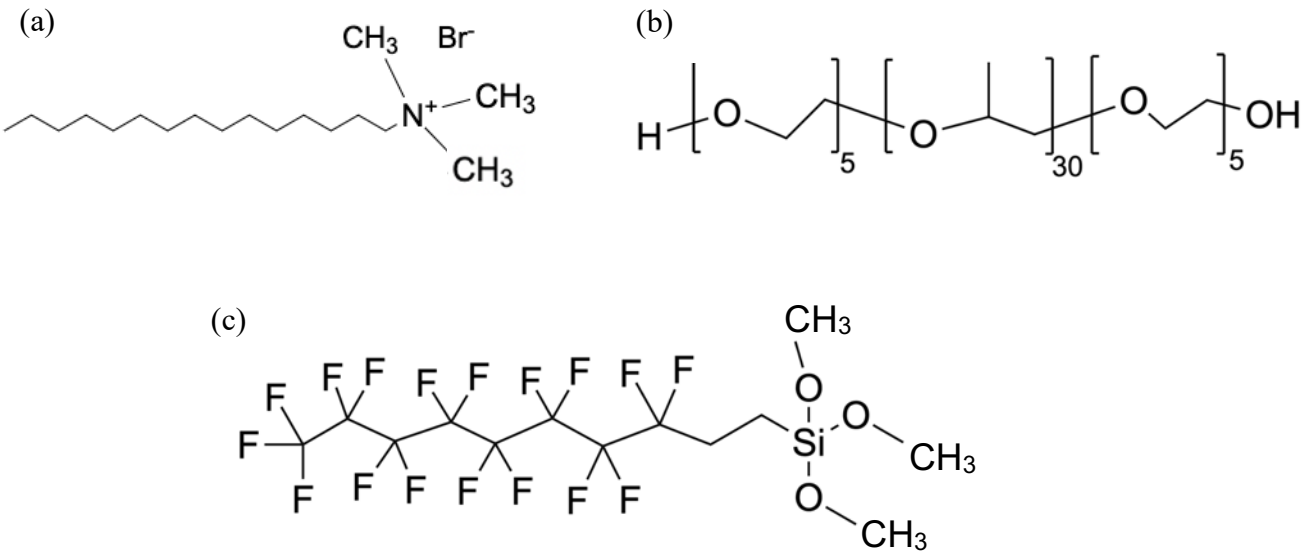

Figure 11: Molecular structures of (a) HTAB, (b) Pluronic L62® and (c) 1H, 1H, 2H, 2H – Perfluorodecyltriethoxysilane

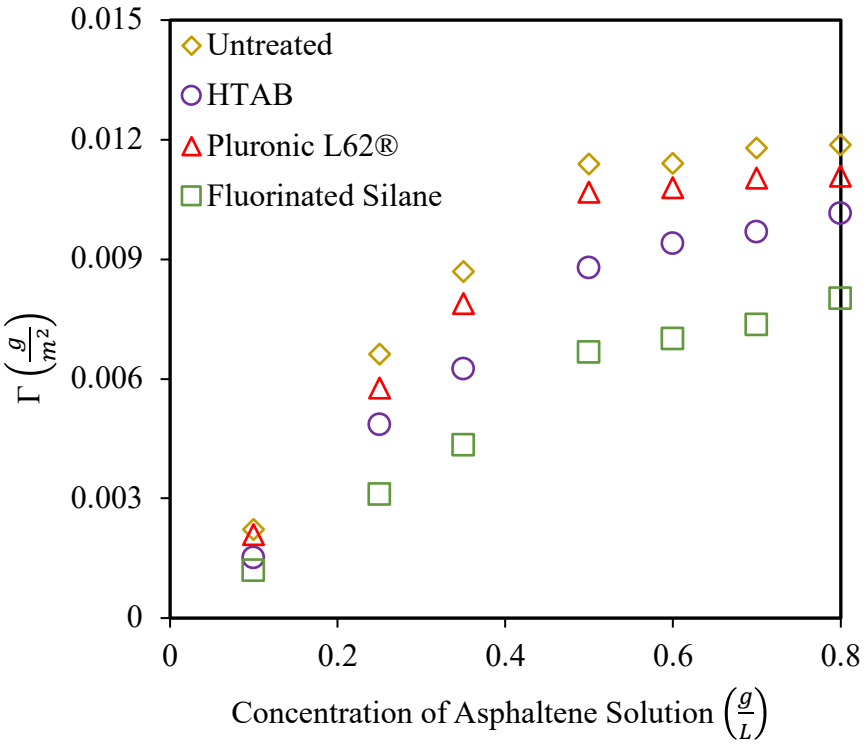

Figure 12: Comparison of asphaltene adsorption onto four different silica surfaces

As can be seen in **Figure 12**, the different surface treatments were able to reduce asphaltene adsorption to varying extents. Of the three surfactants, the fluorinated silane was the most effective in reducing asphaltene adsorption in this concentration range – effecting reductions of up to 40%. While the HTAB and the Pluronic treatments both rendered an alkane surface on the silica particles, the HTAB was almost consistently twice as effective than the Pluronic. This observation is likely to be explained by the differences in their ability to shield the underlying surface from asphaltene interaction through a combined effect of a thicker and more tightly packed hydrophobic coating. Turgman et al. studied the extent of asphaltene adsorptions onto silica that were functionalized with alkyl trichlorosilanes of varying chain lengths and concluded that the extent of asphaltene adsorption was dependent on the SAM carbon chain length and grafting density. At longer chain lengths ($n_c > 16$), the alkyl trichlorosilane undergoes a transition from liquid-like to semicrystalline, increasing the grafting density of these surfactants and in turn increasing overall hydrophobicity of the surface [27,40]. The trend in the ability of a surfactant in reducing asphaltene adsorption seems to be correlated with the hydrophobicity of the functional groups that are exposed to the asphaltene molecules. The hypothesis here is that the adsorption of asphaltene onto untreated silica particles is driven by acid-base interactions between the aromatic cores of the asphaltene molecules and the hydroxide groups on the silica surface. Therefore, as the surface becomes more hydrophobic, due to surface modification, asphaltene would adsorb to a lesser extent.

A wettability study was conducted by measuring the water contact angle onto glass slides functionalized with these three different surfactants to confirm the hydrophobicity trends asserted above. These results are shown in **Figure 12** below. These images were obtained using the FTÅ200 (FTA Instruments; Portsmouth, VA).

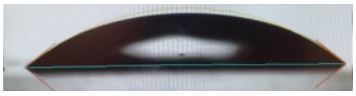

37.5°
(a)

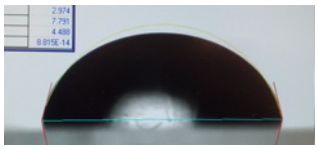

76.8 °
(b)

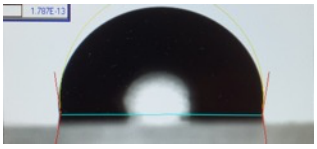

99.2 °
(c)

Figure 13: Contact angles of water onto glass slides functionalized with (a) Pluronic L62®, (b) HTAB and (c) 1H, 1H, 2H, 2H – Perfluorodecyltriethoxysilane.

As can be seen in **Figure 13**, as the water contact angle increases from left to right, the hydrophobicity of the modified surfaces surface increases.

The methodology to obtain the adsorption isotherm in **Section 3.1.1** was repeated for each surface to obtain the Freundlich model parameters for each system, and the results are plotted in **Figure 14**.

Table 3: Freundlich model parameters for each silica surface

Silica Surface	$\boldsymbol{\alpha}$	**β**	$\mathbf{R^2}$
Untreated	0.017	0.81	0.93
HTAB	0.015	0.92	0.96
Pluronic L62®	0.016	0.82	0.94
Fluorinated Silane	0.011	0.93	0.98

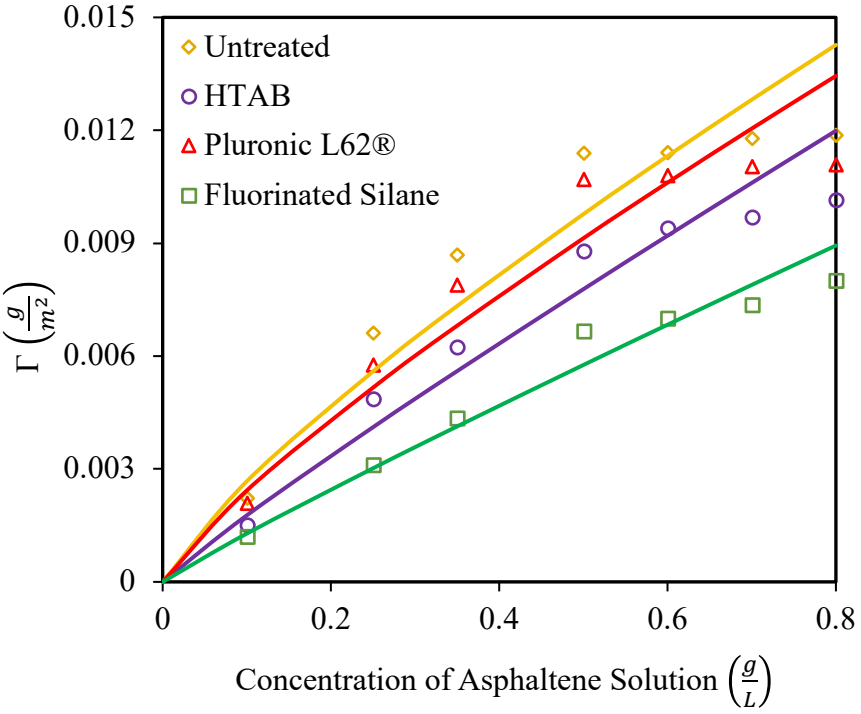

Figure 14: Freundlich isotherms for asphaltene adsorption on the four surfaces investigated

3.2 Asphaltene Deposition Study with Flow System

In this study of asphaltene deposition, flow experiments were performed on a series of asphaltene in 1:1 toluene/tetradecane solutions ranging from 1 to 9 g/L. One g/L was chosen as the lower limit of this concentration range as it was the lowest concentration in which a measurable pressure difference change could be detected using the differential pressure transducer used. The Ergun analysis (as outlined step-by-step in **Appendix 1**) is used to calculate the total mass of asphaltene that deposits onto the column per m^2 of sand surface area available (Γ'). The apostrophe in this case indicates that this quantity measures the mass deposited as opposed to adsorbed onto the silica particles in the column. Since this is a poor solvent for asphaltenes, it can be expected that these solutions contain a both dissolved and undissolved asphaltene species.

3.2.1 Development of the Asphaltene Adlayer on Untreated Silica

The primary data that are collected from these asphaltene deposition experiments are the changes in the pressure drop through the experimental duration, as highlighted in **Figure 6** earlier. **Figure 6** highlights this pressure drop change for the 6 g/L deposition experiment onto untreated silica. The linear increase in the pressure drop across the column is consistent with all of the other deposition experiments. Using Ergun analysis, the decrease in the column porosity and the development of the asphaltene deposition layer (referred to as "adlayer" in the rest of this study) was tracked as a function of time. This layer is assumed to grow radially outward from the surface of each silica particle.

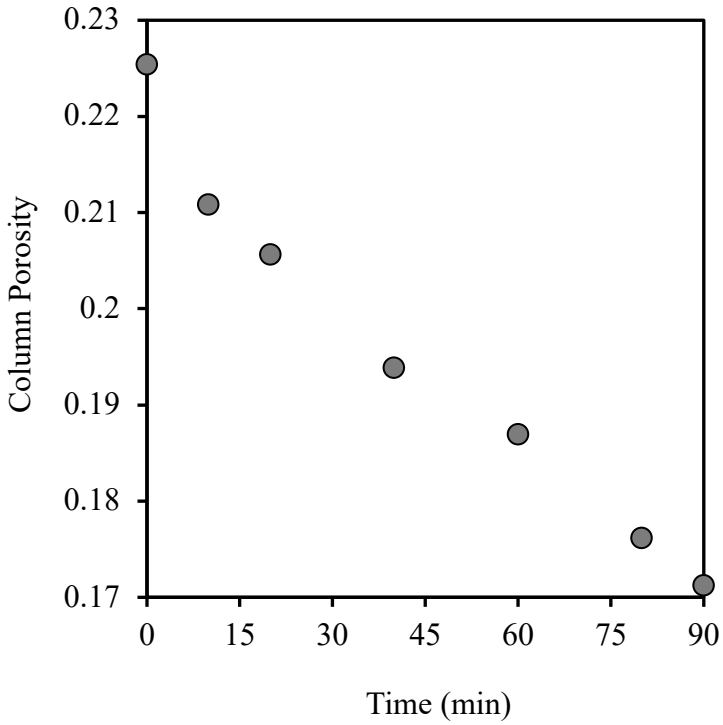

Figure 15: Decrease in the column porosity for the 6 g/L on untreated silica trial

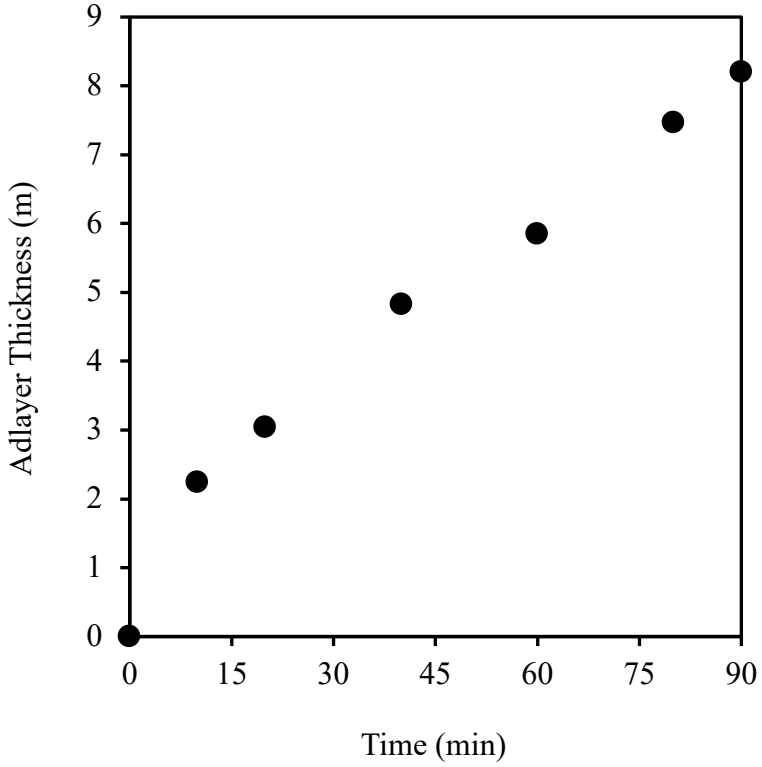

Figure 16: Development of the asphaltene adlayer for the 6 g/L on untreated silica trial

From **Figure 16**, one can see that the development of this asphaltene adlayer is linear, in accordance with the linear decrease in porosity across the packed column. Based on the adlayer thickness at the end of the experiment, which in the 6 g/L on untreated silica case is 8.2 μm, Γ' can be calculated for this trial.

3.2.2 Rate of Mass of Asphaltene Deposited/Unit Area (Γ') Onto Four Silica Surfaces

Figure 16 provides a suitable template to compare the rate of asphaltene deposition across the four different silica surfaces. However, instead of comparing the rate of adlayer development, it would be more appropriate to compare the rate of Γ' development to account for the different masses of sand used in each experiment (due to the different lubricating effects of the surface treatments). The results from the 6 g/L trials on the four surfaces are shown in the figure below.

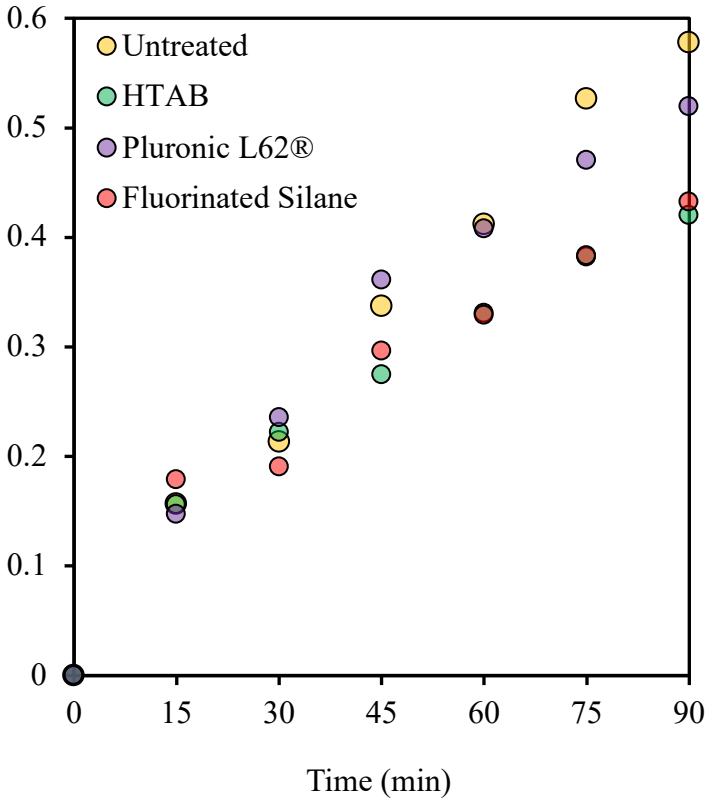

Figure 17: Rate of asphaltene deposition for the 6 g/L trial across the four silica surfaces

One can see from **Figure 17** that the rate of asphaltene deposition is linear as well for the three treated silica surfaces. Surface modification reduces the rate of asphaltene deposition, most notably for the HTAB and fluorinated silane functionalization. At this point, it can be observed that hydrophobic surface modification reduces the asphaltene's ability to deposit onto a particular surface, with the fluorinated silane being able to effect up to a 27% decrease in the rate of deposition at a flow experiment with 6 g/L asphaltene in a 1:1 toluene/tetradecane mixture.

3.2.3 Mass of Asphaltene Deposited/Unit Area (Γ′) Onto Four Silica Surfaces Across Nine Concentrations

By conducting these asphaltene deposition experiments at different concentrations, one can measure the extents of asphaltene deposition (as measured by Γ′) over the fixed period of 90 minutes. The result from these experiments conducted across the four silica surfaces are as shown in **Figure 18**.

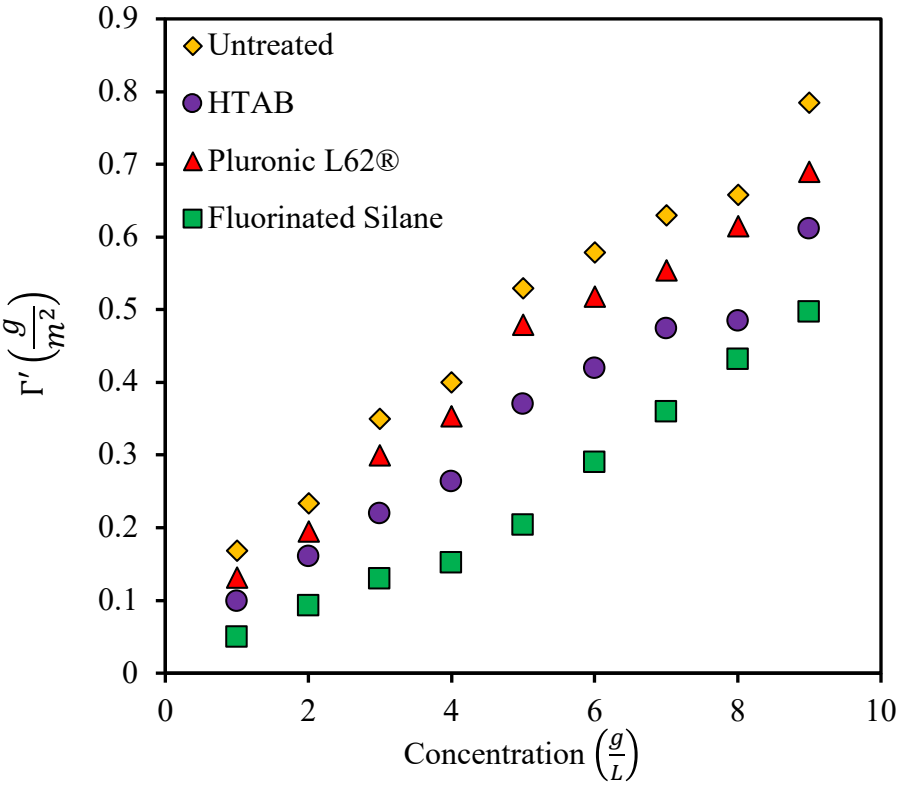

Figure 18: Extent of asphaltene deposition for various asphaltene concentrations onto four types of silica surfaces over 90 min

Looking at the Γ′ value for the 1 g/L trial on untreated silica, it can be deduced that decreasing the solvency of the asphaltenes using tetradecane in the inlet solution increases the mass of asphaltene removed in the column by a factor of ten compared to the 1 g/L asphaltene in toluene experiment conducted over untreated silica. The trend in surface treatment effectiveness in mitigating asphaltene

deposition is equivalent to that observed in the adsorption study – the fluorinated silane was the most effective, followed by HTAB and the least effective is the Pluronic L62®. Throughout this concentration range, there appears to be a linear relationship between Γ′ and the asphaltene concentration for these four silica surfaces. This suggests that asphaltene deposition is not restricted to a monolayer. The fact that asphaltene deposition increases linearly as a function of both time and concentration (as shown in **Figures 17** and **18**) confirm the physical phenomenon of asphaltene buildup in oil pipes, where asphaltene deposition is not restricted to a monolayer and that asphaltene-asphaltene interactions may cause asphaltene aggregates/precipitates to stick onto deposited asphaltene particles.

As the concentration is increased, the volume mean diameter of the precipitated asphaltene "flocks" increases accordingly [41]. In order to evaluate whether the effectiveness of each surface modification is a function of the flock size, we can calculate the percent reduction in Γ′ (using the untreated silica case at that concentration as a basis) for each surface modification trial across the entire concentration range.

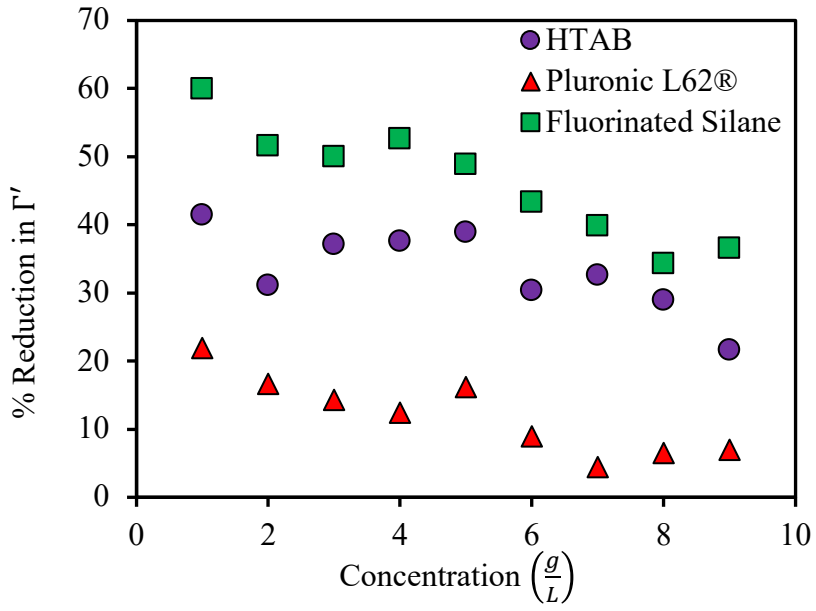

Figure 19: Percent reduction in Γ′ effected by each surface treatment across various asphaltene concentrations

Interestingly, for all 3 surface treatments tested, its effectiveness (as measured by this percentage reduction in Γ') decreases as the concentration of asphaltene is increased. Across this concentration range, each surface modification's effectiveness decreases by about 50%. This suggests that surface modification is less effective in mitigating the deposition of larger asphaltene species and in suppressing asphaltene deposition onto other pre-deposited asphaltene entities.

3.3 Asphaltene Adsorption/Deposition using Quartz Crystal Microbalance (QCM)

The purpose of this QCM study is two-fold: the first is to get more accurate insight into the deposition kinetics of asphaltene onto the surface functionalities tested in the adsorption and deposition experiments, and the second is to see if different measurement methods of measuring asphaltene adsorption/deposition would enable us to reach similar conclusions with respect to surface modification. As described in **Section 2.1**, for the QCM experiment, three gold/quartz crystals were first functionalized using three different SAMs to generate hydroxyl, alkane and fluorine surfaces, respectively. The results of the SAM functionalization experiments are depicted in **Figure 20** below.

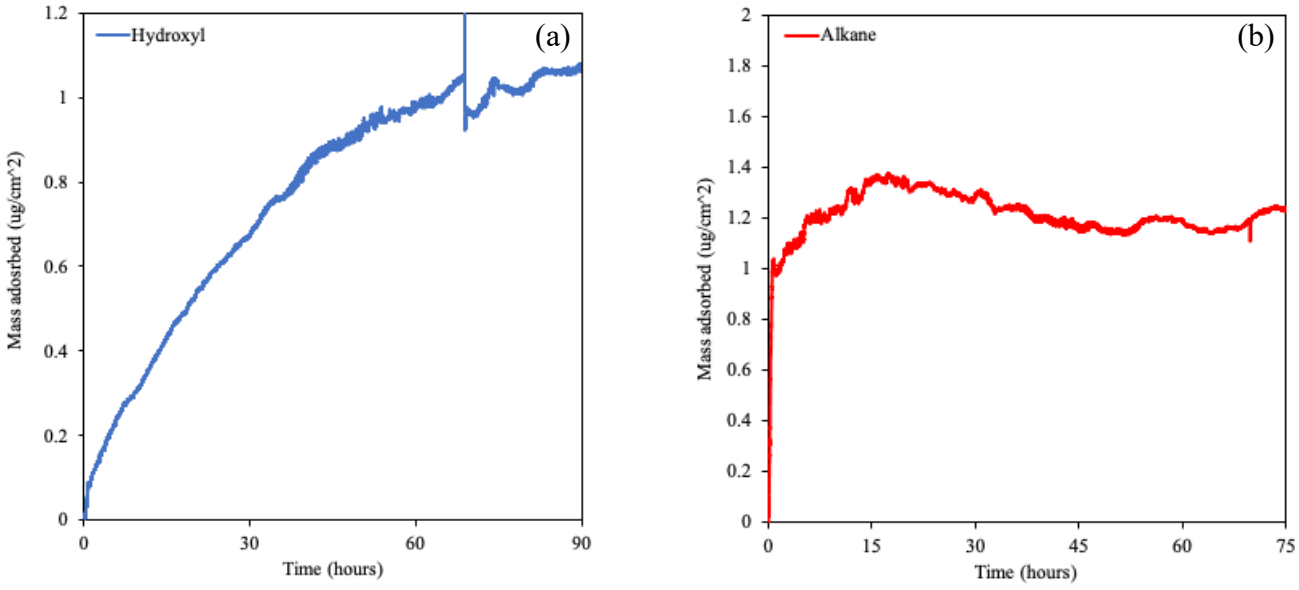

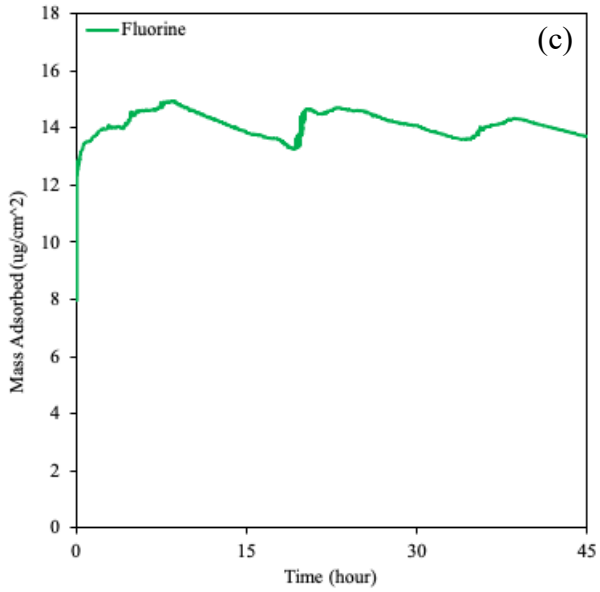

Figure 20: Functionalization of (a) hydroxyl, (b) alkane and (c) fluorine surfaces onto three gold/quartz crystals

It is interesting to note that the SAM assembly times for these different thiols on these gold surfaces range from 15 – 90 hours as shown for the fluorine and hydroxyl cases respectively. Moreover, the hexadecanethiol and 1H, 1H, 2H, 2H – Perfluorodecanethiol exhibits very rapid initial adsorption onto the gold surface, as opposed to a more gradual adsorption process evident with the 2-mercaptoethanol. Secondly, the relative differences in the equilibrium masses of SAMs adsorbed in each of these three cases differ from the relative molar masses of the three thiols used – suggesting different adsorption densities of these SAMs on the gold surface. **Figure 20** suggests that the equilibrium molar adsorption masses are 137, 52.2 and 308 $\frac{\mu mol}{m^2}$ for the hydroxyl, alkane and fluorine-functionalized thiols respectively.

These three gold surfaces were then immersed in a 0.5 g/L solution of asphaltene in toluene/tetradecane. The hydroxyl surface is meant to mimic untreated silica, while the alkane and

fluorine SAM treatments are meant to reflect the alkane and perfluorinated surface modifications conducted in the adsorption and deposition studies.

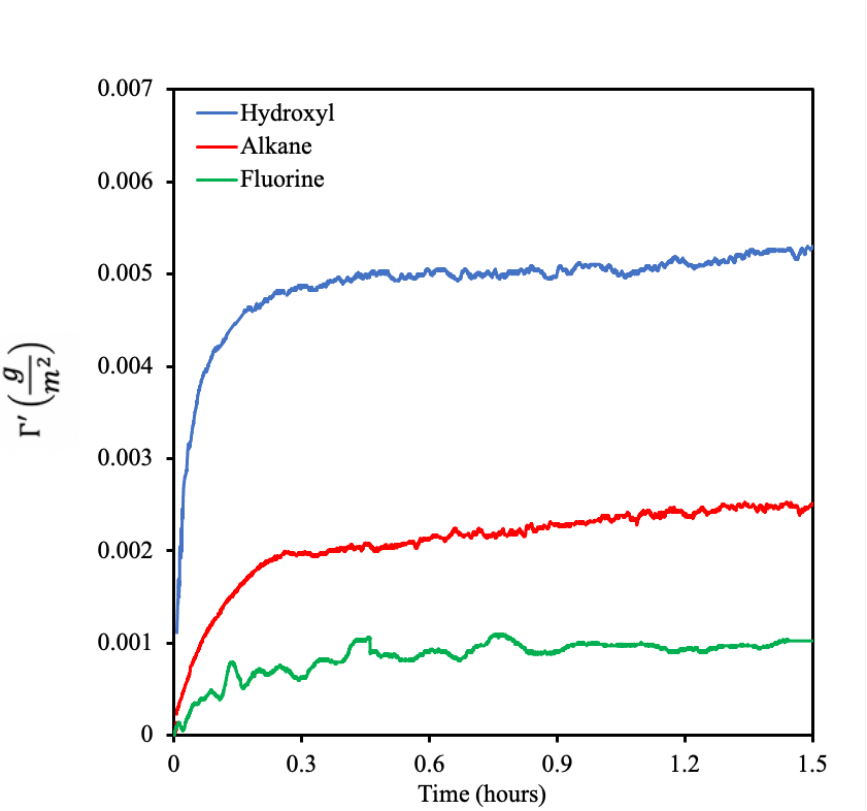

Figure 20: Mass adsorbed/deposited of asphaltene onto three functionalized gold surfaces from a 0.5 g/L asphaltene solution in a 1:1 toluene/tetradecane mixture

Overall, there are no stark differences in the deposition kinetics of asphaltene onto these three surfaces. In terms of the relative effectiveness of the alkane and fluorine surface treatments, the results from this QCM study mirror that of the adsorption and deposition experiments, with the fluorinated functionality being more effective than the alkane functionality in mitigating asphaltene adsorption/deposition. Moreover, the magnitude of the Γ' values observed in these static QCM experiments are substantially less than what would have been observed in the deposition study. Firstly, this highlights the potential significance of inertial impact on asphaltene deposition. Secondly, this also might suggest uneven asphaltene deposition in the deposition study. This might cause particularly large

asphaltene precipitates to lodge in the voids of the packed column, artificially causing a spike in the pressure difference observed – which would render Γ' to be higher than what would have been observed if only asphaltene deposited on the silica particles were considered.

4. Conclusions

Surface modification techniques were shown to decrease the extent of asphaltene adsorption and deposition under dynamic conditions. Out of the three surfactants tested in this study, HTAB, Pluronic L62® and 1H, 1H, 2H, 2H – Perfluorodecyltriethoxysilane, the perfluorinated silane was the most effective in mitigating asphaltene adsorption/deposition. The effectiveness of surface treatment in mitigating asphaltene adsorption and deposition is correlated to the hydrophobicity of the surface groups in contact with the asphaltene molecules in solution. The perfluorinated silane reduced asphaltene adsorption by up to 40% and asphaltene deposition by up to 60%. In the asphaltene deposition study, it was observed that surface modification proved to be less effective in preventing deposition of larger asphaltene entities and deposition of asphaltene particles onto pre-deposited asphaltenes on the silica surface. The magnitude of the mass of asphaltene deposited during the QCM study differed from that from the flow system experiments by a factor of ten, highlighting the importance of inertial impaction in asphaltene deposition.

5. References

(1) Adams, J. J. Asphaltene Adsorption, a Literature Review. *Energy Fuels* **2014**, *28* (5), 2831–2856. https://doi.org/10.1021/ef500282p.

(2) Groenzin, H.; Mullins, O. C. Asphaltene Molecular Size and Structure. *J. Phys. Chem. A* **1999**, *103* (50), 11237–11245. https://doi.org/10.1021/jp992609w.

(3) Shi, Q.; Hou, D.; Chung, K. H.; Xu, C.; Zhao, S.; Zhang, Y. Characterization of Heteroatom Compounds in a Crude Oil and Its Saturates, Aromatics, Resins, and Asphaltenes (SARA) and Non-Basic Nitrogen Fractions Analyzed by Negative-Ion Electrospray Ionization Fourier Transform Ion Cyclotron Resonance Mass Spectrometry. *Energy Fuels* **2010**, *24* (4), 2545–2553. https://doi.org/10.1021/ef901564e.

(4) McKenna, A. M.; Purcell, J. M.; Rodgers, R. P.; Marshall, A. G. Identification of Vanadyl Porphyrins in a Heavy Crude Oil and Raw Asphaltene by Atmospheric Pressure Photoionization Fourier Transform Ion Cyclotron Resonance (FT-ICR) Mass Spectrometry. *Energy Fuels* **2009**, *23* (4), 2122–2128. https://doi.org/10.1021/ef800999e.

(5) *Structures and Dynamics of Asphaltenes*; Mullins, O. C., Sheu, E. Y., Eds.; Springer US, 1998. https://doi.org/10.1007/978-1-4899-1615-0.

(6) Gray, M. R.; Tykwinski, R. R.; Stryker, J. M.; Tan, X. Supramolecular Assembly Model for Aggregation of Petroleum Asphaltenes. *Energy Fuels* **2011**, *25* (7), 3125–3134. https://doi.org/10.1021/ef200654p.

(7) Mullins, O. C. The Modified Yen Model. *Energy Fuels* **2010**, *24* (4), 2179–2207. https://doi.org/10.1021/ef900975e.

(8) Badre, S.; Goncalves, C. C.; Norinaga, K.; Gustavson, G.; Mullins, O. C. Molecular Size and Weight of Asphaltene and Asphaltene Solubility Fractions from Coals, Crude Oils and Bitumen. *Fuel* **2006**, *85* (1), 1–11. https://doi.org/10.1016/j.fuel.2005.05.021.

(9) Andreatta, G.; Goncalves, C. C.; Buffin, G.; Bostrom, N.; Quintella, C. M.; Arteaga-Larios, F.; Pérez, E.; Mullins, O. C. Nanoaggregates and Structure−Function Relations in Asphaltenes. *Energy Fuels* **2005**, *19* (4), 1282–1289. https://doi.org/10.1021/ef0497762.

(10) Mullins, O. C.; Sabbah, H.; Eyssautier, J.; Pomerantz, A. E.; Barré, L.; Andrews, A. B.; Ruiz-Morales, Y.; Mostowfi, F.; McFarlane, R.; Goual, L.; Lepkowicz, R.; Cooper, T.; Orbulescu, J.; Leblanc, R. M.; Edwards, J.; Zare, R. N. Advances in Asphaltene Science and the Yen-Mullins Model. *Energy Fuels* **2012**, *26* (7), 3986–4003. https://doi.org/10.1021/ef300185p.

(11) Al-Hosani, A.; Ravichandran, S.; Daraboina, N. Review of Asphaltene Deposition Modeling in Oil and Gas Production. *Energy Fuels* **2021**, *35* (2), 965–986. https://doi.org/10.1021/acs.energyfuels.0c02981.

(12) Morrow, N. R. Wettability and Its Effect on Oil Recovery. *J. Pet. Technol.* **1990**, *42* (12), 1476–1484. https://doi.org/10.2118/21621-PA.

(13) Melo Faus, F.; Grange, P.; Delmon, B. Influence of Asphaltene Deposition on Catalytic Activity of Cobalt Molybdenum on Alumina Catalysts. *Appl. Catal.* **1984**, *11* (2), 281–293. https://doi.org/10.1016/S0166-9834(00)81886-2.

(14) Mohammed, S.; Gadikota, G. Dynamic Wettability Alteration of Calcite, Silica and Illite Surfaces in Subsurface Environments: A Case Study of Asphaltene Self-Assembly at Solid Interfaces. *Appl. Surf. Sci.* **2020**, *505*, 144516. https://doi.org/10.1016/j.apsusc.2019.144516.

(15) Joonaki, E.; Buckman, J.; Burgass, R.; Tohidi, B. Water versus Asphaltenes; Liquid–Liquid and Solid–Liquid Molecular Interactions Unravel the Mechanisms behind an Improved Oil Recovery Methodology. *Sci. Rep.* **2019**, *9*. https://doi.org/10.1038/s41598-019-47782-5.

(16) Cruz, E. E. B.; Rivas, N. V. G.; García, U. P.; Martinez, A. M. M.; MeloBanda, J. A. *Characterization of Crude Oils and the Precipitated Asphaltenes Fraction Using UV*

Spectroscopy, Dynamic Light Scattering and Microscopy; IntechOpen, 2017. https://doi.org/10.5772/intechopen.70108.

(17) Evdokimov, I. N.; Eliseev, N. Yu.; Akhmetov, B. R. Assembly of Asphaltene Molecular Aggregates as Studied by Near-UV/Visible Spectroscopy: I. Structure of the Absorbance Spectrum. *J. Pet. Sci. Eng.* **2003**, *37* (3), 135–143. https://doi.org/10.1016/S0920-4105(02)00350-9.

(18) Syunyaev, R. Z.; Balabin, R. M.; Akhatov, I. S.; Safieva, J. O. Adsorption of Petroleum Asphaltenes onto Reservoir Rock Sands Studied by Near-Infrared (NIR) Spectroscopy. *Energy Fuels* **2009**, *23* (3), 1230–1236. https://doi.org/10.1021/ef8006068.

(19) Dudášová, D.; Silset, A.; Sjöblom, J. Quartz Crystal Microbalance Monitoring of Asphaltene Adsorption/Deposition. *J. Dispers. Sci. Technol.* **2008**, *29* (1), 139–146. https://doi.org/10.1080/01932690701688904.

(20) Hu, X.; Yutkin, M. P.; Hassan, S.; Wu, J.; Prausnitz, J. M.; Radke, C. J. Asphaltene Adsorption from Toluene onto Silica through Thin Water Layers. *Langmuir* **2019**, *35* (2), 428–434. https://doi.org/10.1021/acs.langmuir.8b03835.

(21) Alkafeef, S. F.; Al-Marri, S. S. Kinetics and Isotherms of Asphaltene Adsorption in Narrow Pores. *Curr. Opin. Colloid Interface Sci.* **2016**, *24*, 44–51. https://doi.org/10.1016/j.cocis.2016.06.005.

(22) Alkafeef, S.; Smith, A. Asphaltene Adsorption Isotherm in the Pores of Reservoir Rock Cores. *Proc. - SPE Int. Symp. Oilfield Chem.* **2005**. https://doi.org/10.2118/93188-MS.

(23) Pernyeszi, T.; Patzkó, Á.; Berkesi, O.; Dékány, I. Asphaltene Adsorption on Clays and Crude Oil Reservoir Rocks. *Colloids Surf. Physicochem. Eng. Asp.* **1998**, *137* (1), 373–384. https://doi.org/10.1016/S0927-7757(98)00214-3.

(24) Marczewski, A. W.; Szymula, M. Adsorption of Asphaltenes from Toluene on Mineral Surface. *Colloids Surf. Physicochem. Eng. Asp.* **2002**, *208* (1), 259–266. https://doi.org/10.1016/S0927-7757(02)00152-8.

(25) Ekholm, P.; Blomberg, E.; Claesson, P.; Auflem, I. H.; Sjöblom, J.; Kornfeldt, A. A Quartz Crystal Microbalance Study of the Adsorption of Asphaltenes and Resins onto a Hydrophilic Surface. *J. Colloid Interface Sci.* **2002**, *247* (2), 342–350. https://doi.org/10.1006/jcis.2002.8122.

(26) Dudášová, D.; Simon, S.; Hemmingsen, P. V.; Sjöblom, J. Study of Asphaltenes Adsorption onto Different Minerals and Clays: Part 1. Experimental Adsorption with UV Depletion Detection. *Colloids Surf. Physicochem. Eng. Asp.* **2008**, *317* (1), 1–9. https://doi.org/10.1016/j.colsurfa.2007.09.023.

(27) Turgman-Cohen, S.; Fischer, D. A.; Kilpatrick, P. K.; Genzer, J. Asphaltene Adsorption onto Self-Assembled Monolayers of Alkyltrichlorosilanes of Varying Chain Length. *ACS Appl. Mater. Interfaces* **2009**, *1* (6), 1347–1357. https://doi.org/10.1021/am900203u.

(28) Girard, H.-L.; Bourrianne, P.; Chen, D.; Jaishankar, A.; Vreeland, J. L.; Cohen, R. E.; Varanasi, K. K.; McKinley, G. H. Asphaltene Adsorption on Functionalized Solids. *Langmuir* **2020**, *36* (14), 3894–3902. https://doi.org/10.1021/acs.langmuir.0c00029.

(29) D04 Committee. *Test Method for N-Heptane Insolubles*; ASTM International. https://doi.org/10.1520/D3279-19.

(30) Berg, J. C. *An Introduction to Interfaces & Colloids: The Bridge to Nanoscience*; World Scientific, Singapore, 2010.

(31) Salunkhe, A. A.; Overney, R. M.; Berg, J. C. The Use of Boundary Lubricants for the Reduction of Shear Thickening and Jamming in Abrasive Particle Slurries. *Colloids Surf. Physicochem. Eng. Asp.* **2018**, *537*, 13–19. https://doi.org/10.1016/j.colsurfa.2017.09.029.

(32) Gelest, Inc. *Silicon Compounds: Silanes and Silicones*, 2nd ed.; 2008.

(33) Alkafeef, S. F.; Gochin, R. J.; Smith, A. L. Measurement of the Electrokinetic Potential at Reservoir Rock Surfaces Avoiding the Effect of Surface Conductivity. *Colloids Surf. Physicochem. Eng. Asp.* **1999**, *159* (2), 263–270. https://doi.org/10.1016/S0927-7757(99)00263-0.
(34) Stanford Research Systems. *QCM200: Quartz Crystal Microbalance Digital Controller*; 2018.
(35) Bird, R. B.; Steward, W. E.; Lightfoot, E. N. *Transport Phenomena*, 2nd ed.; John Wiley & Sons, INc., 2007.
(36) Kankare, J. Sauerbrey Equation of Quartz Crystal Microbalance in Liquid Medium. *Langmuir* **2002**, *18* (18), 7092–7094. https://doi.org/10.1021/la025911w.
(37) Swenson, H.; Stadie, N. P. Langmuir's Theory of Adsorption: A Centennial Review. *Langmuir* **2019**, *35* (16), 5409–5426. https://doi.org/10.1021/acs.langmuir.9b00154.
(38) Acevedo, S.; Castillo, J.; Fernández, A.; Goncalves, S.; Ranaudo, M. A. A Study of Multilayer Adsorption of Asphaltenes on Glass Surfaces by Photothermal Surface Deformation. Relation of This Adsorption to Aggregate Formation in Solution. *Energy Fuels* **1998**, *12* (2), 386–390. https://doi.org/10.1021/ef970152o.
(39) Duong, A.; Smith, K. J. A Model of Ceramic Membrane Fouling during Heavy Oil Ultrafiltration. *Can. J. Chem. Eng.* **1997**, *75* (6), 1122–1129. https://doi.org/10.1002/cjce.5450750616.
(40) Smith, M. B.; Efimenko, K.; Fischer, D. A.; Lappi, S. E.; Kilpatrick, P. K.; Genzer, J. Study of the Packing Density and Molecular Orientation of Bimolecular Self-Assembled Monolayers of Aromatic and Aliphatic Organosilanes on Silica. *Langmuir* **2007**, *23* (2), 673–683. https://doi.org/10.1021/la062475v.
(41) Rastegari, K.; Svrcek, W. Y.; Yarranton, H. W. Kinetics of Asphaltene Flocculation. *Ind. Eng. Chem. Res.* **2004**, *43* (21), 6861–6870. https://doi.org/10.1021/ie049594v.

Appendix 1: Calculating Adlayer Thickness (δ) and Mass Deposited/unit area (Γ') using Ergun Analysis (6 g/L asphaltene in 1:1 toluene/tetradecane solution on untreated silica)

Sand Properties:

- Mass of Sand in column = 7.3785 g
- Density of Sand = 2500 $\frac{kg}{m^3}$
- Surface Area available of sand = 0.0579 $\frac{m^2}{g}$

Column Properties:

- Column Length = 0.099 m
- Diameter of Column = 0.007 m
- $\Delta P_{initial} = 0.091\ psi$
- $\Delta P_{final} = 0.227\ psi$

} Obtained from **Figure 4**

Fluid properties:

- Concentration of Asphaltene in toluene/tetradecane solution = 6 $\frac{g}{L}$
- Density of asphaltene solution = 803.7 $\frac{\text{kg}}{m^3}$
- Density of Asphaltene = 1200 $\frac{kg}{m^3}$
- Viscosity of solution = 0.00096 $Pa \cdot s$
- Volumetric flow rate = 1 ml/min = $1.667 * 10^{-8}\ \frac{m^3}{s}$

Derived Quantities (from Column/Flow Physical Properties):

- Column Cross-sectional Area:

$$A_{cross\ section} = \pi * \left(\frac{D}{2}\right)^2 = \pi * (0.007\ m)^2 = 3.85 * 10^{-5}\ m^2$$

- Superficial Fluid Velocity

$$v_o = \frac{V}{A_{cross\ section}} = \frac{1.667 * 10^{-8}\ \frac{m^3}{s}}{3.85 * 10^{-5}\ m^2} = 4.33 * 10^{-4}\ \frac{m}{s}$$

Step 1: Calculate $\varepsilon_{initial}$(Initial Porosity) of the Packed Column after packing it with sand

In this step, we will be determining the $\varepsilon_{initial}$ of the packed column by taking into account how much sand is packed into the column.

Volume of sand used in the experiment,

$$V_{sand} = \frac{M_{sand}}{\rho_{sand}} = \frac{7.3785\ g}{2{,}500{,}000\ g/m^3} = 2.95 * 10^{-6}\ m^3$$

Volume of empty column,

$$A_{cross\ section} * Column\ Length = 3.85 * 10^{-5}\ m^2 * 0.099\ m = 3.81 * 10^{-6}\ m^3$$

∴ Starting Column Porosity

$$\varepsilon_{initial} = \frac{V_{empty\ column} - V_{sand}}{V_{empty\ column}} = \frac{3.81 * 10^{-6}\ m^3 - 2.95 * 10^{-6}\ m^3}{3.81 * 10^{-6} m^3} = 0.225$$

Step 2: Calculate $D_{p,initial}$ (Average Initial Diameter) of Each Particle

Here, we will be determining the average initial diameter of each sand particle ($D_{p,initial}$) by solving the Ergun equation numerically using the pre-experiment column and flow properties.

Initial Ergun Eq left-hand side,

$$\frac{\Delta P_{initial}}{L} = 0.091\ psi * \frac{6894.76\ Pa}{1\ psi} * \frac{1}{0.099\ m} = \ 6337.59\ \frac{Pa}{m}$$

Initial Ergun Eq right-hand side,

$$\ldots = 150\left(\frac{\mu v_o}{D_{p,initial}^2}\right)\frac{(1-\varepsilon_{initial})^2}{\varepsilon_{initial}^3} + \frac{7}{4}\left(\frac{\rho v_o^2}{D_{p,initial}}\right)\frac{1-\varepsilon_{initial}}{\varepsilon_{initial}^3}$$

$$\ldots = 150\left(\frac{0.000961\ Pa\cdot s\ * 4.33 * 10^{-4}\ \frac{m}{s}}{D_{p,initial}^2}\right)\frac{(1-0.225)^2}{0.225^3} + \frac{7}{4}\left(\frac{815\frac{kg}{m^3}\ *\left(4.33 * 10^{-4}\ \frac{m}{s}\right)^2}{D_{p,intiial}}\right)\frac{1-0.225}{0.225^3}$$

∴ To solve for D_p, set the left-hand side equal to right-hand side

$$6337.59\frac{Pa}{m} = \ 150\left(\frac{0.000961\ Pa\cdot s\ * 4.33 * 10^{-4}\ \frac{m}{s}}{D_{p,initial}^2}\right)\frac{(1-0.225)^2}{0.225^3} + \frac{7}{4}\left(\frac{815\frac{kg}{m^3}\ *\left(4.33 * 10^{-4}\ \frac{m}{s}\right)^2}{D_{p,intiial}}\right)\frac{1-0.225}{0.225^3}$$

➔ Using Mathematica/Solver

$$D_{p,initial} = 0.00072\ m = \ 0.72\ \text{mm} \leftarrow$$

Step 3: Rewriting $D_{p,final}$ and ε_{final} in terms of δ(Adlayer thickness), $D_{p,initial}$ and $\varepsilon_{initial}$

The goal of this step is to rewrite the 2 variables $D_{p,final}$ and ε_{final} solely in terms of the initial column properties and δ so that in the next step, we would only have 1 equation (Ergun equation involving the column properties at the end of the experiment), and one unknown, δ.

The primary assumption made in the following calculation is that asphaltene deposition is **uniform** and deposits as a **concentric, spherical layer** on top of each silica particle.

$D_{p,final}$ (final particle diameter after asphaltene deposition) can be written as,

$$D_{p,final} = D_{p,initial} + 2\delta$$

$$D_{p,final} = 0.00072\ m + 2\delta \leftarrow$$

ε_{final} (final column porosity after asphaltene deposition) can be written as,

$$\varepsilon_{final} = \frac{V_{empty\ column} - V_{sand\ with\ asphaltene\ deposited\ on}}{V_{empty\ column}}$$

$$V_{sand\ with\ asphaltene\ deposited\ on} = Number\ of\ Sand\ Particles * \frac{New\ Volume}{Sand\ Particle}$$

$$Number\ of\ Sand\ Particles = \frac{V_{sand}\ (from\ step\ 1)}{V_{sand\ particle\ before\ asphaltene\ deposition}}$$

$$= \frac{V_{sand}\ (from\ step\ 1)}{\frac{4}{3}\pi\left(\frac{D_{p,initial}\ (from\ step\ 2)}{2}\right)^3}$$

$$= \frac{2.95 * 10^{-6}\ m^3}{\frac{4}{3}\pi\left(\frac{0.00072\ m}{2}\right)^3}$$

$$\approx\ 15{,}095\ particles$$

$$\frac{New\ Volume}{Sand\ Particle} = \frac{4}{3}\pi\left(\frac{D_{p,final} + 2\delta}{2}\right)^3 = \frac{4}{3}\pi\left(\frac{0.00072\ m + 2\delta}{2}\right)^3$$

$$V_{sand\ with\ asphaltene\ deposited\ on} = 15{,}095\ particles * \frac{4}{3}\pi\left(\frac{0.00072\ m + 2\delta}{2}\right)^3$$

$$\varepsilon_{final} = \frac{V_{empty\ column} - 15{,}095\ particles * \frac{4}{3}\pi\left(\frac{0.00072\ m + 2\delta}{2}\right)^3}{V_{empty\ column}}$$

$$\varepsilon_{final} = \frac{3.81 * 10^{-6}\ m^3 - 15{,}095\ particles * \frac{4}{3}\pi\left(\frac{0.00072\ m + 2\delta}{2}\right)^3}{3.81 * 10^{-6}\ m^3}$$

Step 4: Solving for δ using the Ergun Analysis using final column properties

Left-hand side of Ergun Equation,

$$\frac{\Delta P_{final}}{L} = 0.227\ psi * \frac{6894.76\ Pa}{1\ psi} * \frac{1}{0.099\ m} = \ 15{,}809.16\ \frac{Pa}{m}$$

Right-hand side of Ergun Equation,

$$\ldots = 150\left(\frac{\mu v_o}{D_{p,final}^2}\right)\frac{\left(1-\varepsilon_{final}\right)^2}{\varepsilon_{final}^3} + \frac{7}{4}\left(\frac{\rho v_o^2}{D_{p,final}}\right)\frac{1-\varepsilon_{final}}{\varepsilon_{final}^3}$$

where from Step 3, we have solved for expressions for

$$D_{p,final} = 0.00072\ m + 2\delta$$

$$\varepsilon_{final} = \frac{3.81 * 10^{-6}\ m^3 - \ 15{,}095\ particles * \frac{4}{3}\pi\left(\frac{0.00072\ m + 2\delta}{2}\right)^3}{3.81 * 10^{-6}\ m^3}$$

➔ Using Mathematica/Solver

$$\delta = 8.2 * 10^{-6}\ m = \ 8.2\ \mu m \leftarrow$$

Step 5: Calculating Γ′ (mass adsorbed/deposited per m^2 of silica)

From the δ calculated from Step 4, we can calculate ε_{final} (final column porosity)

$$\varepsilon_{final} = \frac{3.81 * 10^{-6}\, m^3 - 15{,}095\, particles * \frac{4}{3}\pi \left(\frac{0.00072\, m + 2\delta}{2}\right)^3}{3.81 * 10^{-6}\, m^3}$$

$$\varepsilon_{final} = 0.171$$

Volume of Asphaltene Deposited,

$$V_{asphaltene\ deposited} = (\varepsilon_{initial} - \varepsilon_{final}) * V_{empty\ column}$$

$$= (0.225 - 0.171) * 3.81 * 10^{-6}\, m^3$$

$$= 2.06 * 10^{-7}\, m^3$$

Γ′ can then be calculated as,

$$\Gamma' = \frac{M_{asphaltene\ deposited}}{Total\ Surface\ Area\ of\ Sand\ Available\ for\ Adsorption}$$

$$\Gamma' = \frac{V_{asphaltene\ deposited} * \rho_{asphaltene}}{M_{sand} * \frac{surface\ area\ of\ sand}{gram\ of\ sand}}$$

$$\Gamma' = \frac{1.65 * 10^{-7}\, m^3 * 1200\, \frac{kg}{m^3}}{7.3785 g * 0.0579\, \frac{m^2}{g}}$$

$$\Gamma' = 0.58 \frac{g}{m^2}$$